

# Empirically Derived Sensitivity of Vegetation to Climate across Global Gradients of Temperature and Precipitation

GREGORY R. QUETIN

*Department of Atmospheric Sciences, University of Washington, Seattle, Washington*

ABIGAIL L. S. SWANN

*Department of Atmospheric Sciences, and Department of Biology, University of Washington, Seattle, Washington*

(Manuscript received 18 November 2016, in final form 10 April 2017)

## ABSTRACT


The natural composition of terrestrial ecosystems can be shaped by climate to take advantage of local environmental conditions. Ecosystem functioning (e.g., interaction between photosynthesis and temperature) can also acclimate to different climatological states. The combination of these two factors thus determines ecological–climate interactions. A global empirical map of the sensitivity of vegetation to climate is derived using the response of satellite-observed greenness to interannual variations in temperature and precipitation. Mechanisms constraining ecosystem functioning are inferred by analyzing how the sensitivity of vegetation to climate varies across climate space. Analysis yields empirical evidence for multiple physical and biological mediators of the sensitivity of vegetation to climate at large spatial scales. In hot and wet locations, vegetation is greener in warmer years despite temperatures likely exceeding thermally optimum conditions. However, sunlight generally increases during warmer years, suggesting that the increased stress from higher atmospheric water demand is offset by higher rates of photosynthesis. The sensitivity of vegetation transitions in sign (greener when warmer or drier to greener when cooler or wetter) along an emergent line in climate space with a slope of about  $59 \text{ mm yr}^{-1} \text{ }^{\circ}\text{C}^{-1}$ , twice as steep as contours of aridity. The mismatch between these slopes is evidence at a global scale of the limitation of both water supply due to inefficiencies in plant access to rainfall and plant physiological responses to atmospheric water demand. This empirical pattern can provide a functional constraint for process-based models, helping to improve predictions of the global-scale response of vegetation to a changing climate.

## 1. Introduction

The structure and productivity of vegetation across the world is coupled to climate through environmental variables such as light, water, and temperature. Structure and productivity of vegetation are also controls on the terrestrial carbon cycle (Friedlingstein et al. 2006), the terrestrial hydrological cycle (Schlesinger and Jasechko 2014; Jasechko et al. 2013), and the surface energy budget (Ghimire et al. 2014). To understand how global vegetation will be altered under climate change, we must understand how ecological–climate interaction operates at large spatial scales and thus across global climate

gradients. In our work we have chosen mean annual temperature and precipitation as climate gradients with historical context in studying vegetation (e.g., Whittaker 1970), related to environmental resources important for vegetation function and with strong variation across the globe (Whittaker 1962; Kottek et al. 2006; Metzger et al. 2013). There is evidence that an important part of the way that vegetation and climate interact is through changes in phenology (Richardson et al. 2010, 2013). Though our analysis aggregates across the seasonal cycle of vegetation and climate, we still observe these changes as interannual variation in the annual means (e.g., a longer growing season is a greener year).

Three common approaches have previously been used to study how vegetation is controlled by the climate of a region and to predict how it will change in the future: 1) climate-biome classification—treating the current boundaries between biomes as determined by climate (Peel et al. 2007; Kottek et al. 2006; Smith et al. 2002;

 Denotes content that is immediately available upon publication as open access.

*Corresponding author:* Gregory R. Quetin, gquetin@u.washington.edu

DOI: 10.1175/JCLI-D-16-0829.1

© 2017 American Meteorological Society. For information regarding reuse of this content and general copyright information, consult the [AMS Copyright Policy](http://www.ametsoc.org/PUBSReuseLicenses) ([www.ametsoc.org/PUBSReuseLicenses](http://www.ametsoc.org/PUBSReuseLicenses)).

Metzger et al. 2013); 2) simplified models of climate constraint—based on physiological constraints on net primary productivity (Churkina and Running 1998; Nemani et al. 2003; Jolly et al. 2005; Running et al. 2004); and 3) global process-based models—extending plant- or plot-scale research to global scales through process-based numerical global models (Oleson et al. 2010; Boisvenue and Running 2006; Levis 2010).

Our analysis serves to bridge the static geographical observational (approach 1) and modeling approaches (approaches 2 and 3) by empirically quantifying the sensitivity of vegetation to interannual variations in environmental variables across the globe. By analyzing these sensitivities across climate space we can diagnose how ecosystem function varies across annual climate and hypothesize mechanisms that could explain the observed pattern. We define ecosystem function here as the integrated environmental modulation of both plant-scale physiological (photosynthesis, respiration, transpiration, and hydraulic stress) and population-scale ecological (demography, disturbance, and competition) processes measured at a coarse spatial scale (100 km  $\times$  100 km). We do not discriminate grid points based on plant type or human influence. Differences in the growth cycle of vegetation that extend into the interannual variations of the vegetation are treated as additional error in our analysis. Our study captures broad patterns of ecosystem functioning across the global range of two environmental conditions (mean annual temperature and precipitation) and allows us to identify major climate constraints on remotely sensed vegetation.

The effect of climate on vegetation is evident from observations of how vegetation is distributed across the globe and is explicit in efforts to classify biomes and the use of climate envelopes to predict the movement of biomes due to climate change (Koven 2013; Rubel and Kottek 2010). However, the way that ecosystem function varies across climate, rather than just vegetation distribution, has not been empirically investigated at a global scale. In this study we combine the concept from climate classification that climate shapes vegetation with our calculation of the interannual sensitivity of vegetation to climate from remotely sensed vegetation and observations and reanalysis of climate data. This allows us to identify emergent functional constraints measured at the scales and resolutions required to make global predictions about vegetation. Analyzing the sensitivity of vegetation across climate space expands on other work and enables us to find the underlying pattern of ecosystem function across global climate gradients (Seddon et al. 2016; Wu et al. 2015). Here our concept of binning across climate space is similar to the common practice in climate science of calculating the zonal mean of a variable, with latitude replaced with temperature and precipitation (see methods) (see Figs. 1 and 4).

## 2. Methods

### a. Empirical sensitivity of vegetation to climate

We create an empirical estimate of the sensitivity of vegetation to climate at global scales by combining the satellite record of the normalized difference vegetation index (NDVI) with globally gridded estimates of temperature and precipitation. NDVI represents the longest global time series available to study vegetation response at a scale commensurate with global carbon cycling and ecological–climate feedbacks (Pinzon and Tucker 2014). NDVI has frequently been used to study temporal trends in vegetated land cover (e.g., Chen et al. 2014) and has been correlated with environmental variables across biomes and regions to demonstrate the connection between the physical environment and surface greenness (Wu et al. 2015; Zhou et al. 2003, 2001; Goward et al. 1991; Asner et al. 2000; Xu et al. 2014; Myneni et al. 2002). Though a simple metric of vegetation, observations of NDVI have the longest continuous global time series and relates strongly to leaf area, fraction of absorbed photosynthetically available radiation, plant fluorescence, gross primary productivity, and more advanced vegetation indices (Myneni et al. 2002; Frankenberg et al. 2011; Guanter et al. 2012; Glenn et al. 2008; Huete et al. 2002). As the time series of MODIS enhanced vegetation index (less saturation in dense vegetation) and targeted measurements of solar-induced fluorescence (a remote observation thought to be proportional to GPP) concurrent with climate observations grow longer we hope to be able to further test many of the hypotheses presented in this paper (Huete et al. 2002; Frankenberg et al. 2014, 2013, 2011; Guanter et al. 2012). In addition to remote sensing, individual flux tower locations can make more direct measurements of carbon and water fluxes (Baldocchi 2014). However, global products derived from these site-level observations (e.g., Jung et al. 2011; Beer et al. 2010; Xiao et al. 2011) also depend heavily on similar satellite observations.

Here we use the globally observed NDVI as a direct observation of greenness to create a metric of ecological–climate interaction. Our analysis uses a multilinear least squares regression between the interannual percentage anomalies in NDVI  $\% \Delta_{\text{NDVI}}$  and the interannual time series of temperature  $T$  in  $^{\circ}\text{C}$  and precipitation  $P$  in  $\text{mm yr}^{-1}$  to determine the sensitivity of greenness to climate at each vegetated grid point of the globe (MATLAB function regress.m) [Eq. (1)]:

$$\% \Delta_{\text{NDVI}} = T\beta_{\text{TEMP}} + P\beta_{\text{PRECIP}} + \beta_0. \quad (1)$$

We interpret the resulting  $\beta_{\text{TEMP}}$  and  $\beta_{\text{PRECIP}}$  for each grid point as the sensitivity of vegetation to interannual

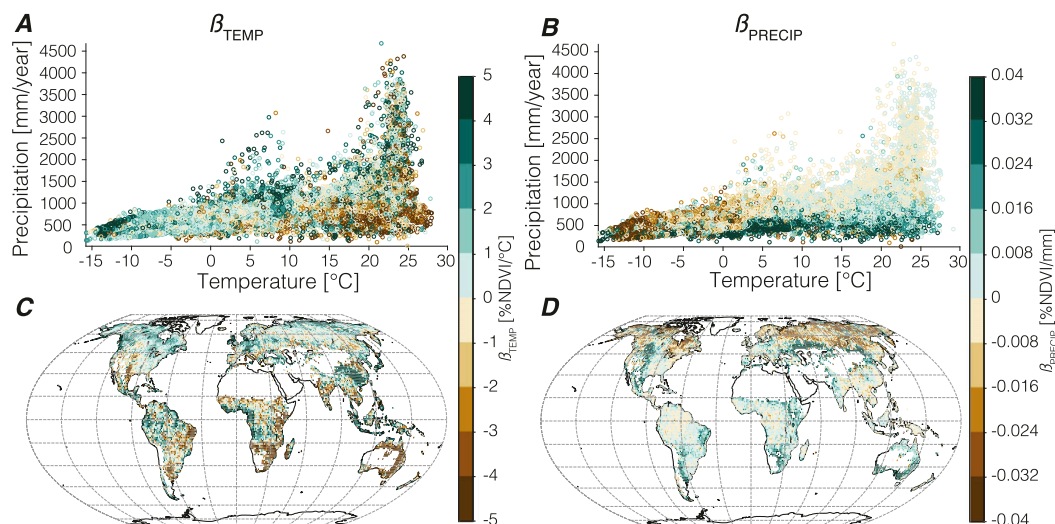


FIG. 1. Sensitivity of vegetation to interannual variation in (a) temperature  $\beta_{TEMP}$  and (b) precipitation  $\beta_{PRECIP}$  calculated from robust regressions for years 1997–2012. Shades of green show positive sensitivity [generally greener vegetation when (a) warmer or (b) wetter]. Shades of brown show negative sensitivity [greener vegetation when (a) cooler or (b) drier]. A map of (c)  $\beta_{TEMP}$  and (d)  $\beta_{PRECIP}$ .

variation of climate. The  $\beta$  terms are expressed as a percent change in the mean NDVI from 1982 to 2012, with units of  $\%NDVI^{\circ}C^{-1}$  and  $\%NDVImm^{-1}$ , respectively. Because of the assumed linear relationship between climate and vegetation implicit in a multilinear regression the coefficients  $\beta_{TEMP}$  and  $\beta_{PRECIP}$  can be interpreted as linearized metrics of ecosystem function. Ecosystem function is not necessarily linear in time or space, but at the limit of the interannual variation and the extent of each bin a linear fit is a useful approximation. In addition, we note that observations of greenness relate most directly to processes and structure of the vegetation canopy. A positive  $\beta$  shows positive sensitivity of vegetation to climate (i.e., greener in a warmer or wetter year), while a negative  $\beta$  shows negative sensitivity of vegetation to climate (i.e., greener in a cooler or drier year).

We chose a simple linear model with two predictors in order to learn about ecosystem–climate interactions from the variation of a metric that reflects ecosystem–climate interactions across climate space. Rather than attempt to create the best linear model for NDVI at each pixel on the map, our regression model serves to linearize the effect of both temperature and precipitation consistently across the globe and simplify interpretation of the results.

Collinearity between the predictor variables of the linear regression (temperature and precipitation) is present at various levels across the globe. However, levels of correlation were not found to exceed commonly cited thresholds that would damage a linear

regression at most grid points, and experiments that excluded high correlation values ( $>0.6$ ) did not impact the results of the analysis (see [appendix](#), section d).

To examine the aggregated structure of  $\beta_{TEMP}$  and  $\beta_{PRECIP}$  across climate space we assign each geospatial point to a bin dictated by its climatological mean annual temperature and precipitation (Figs. 1 and 2). The pattern of aggregated  $\beta_{TEMP}$  and  $\beta_{PRECIP}$  across climate contains information about climate and ecological–climate interactions allowing us to hypothesize what physiological mechanisms are responsible for how climate shapes each ecosystem. For example,  $\beta_{TEMP}$  is likely influenced by interannual variations in photosynthetic performance due to chemical rates (Berry and

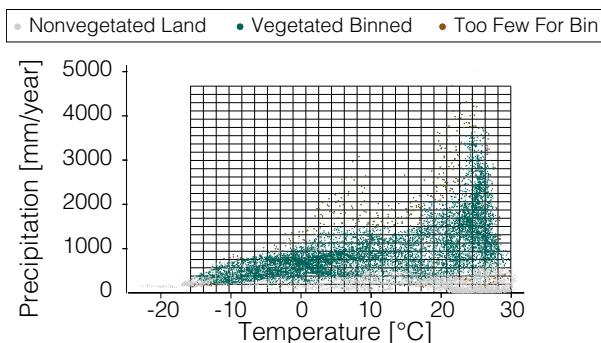


FIG. 2. Spatial points plotted in climate space of mean annual temperature and mean annual precipitation. Nonvegetated grid points (gray), vegetated grid points used in analysis (green), and vegetated grid points where there were fewer than 10 in a bin (brown).

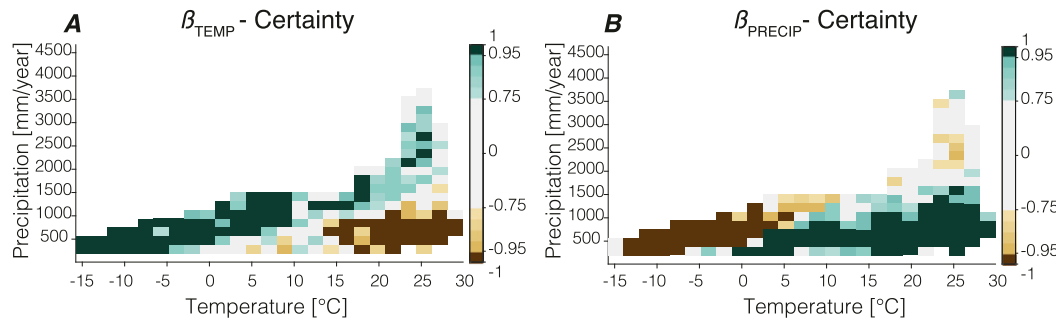


FIG. 3. Combined temporal and spatial uncertainty for bins of (a)  $\beta_{\text{TEMP}}$  and (b)  $\beta_{\text{PRECIP}}$ . Dark colors show bins with 95% confidence that average is greater than (green) or less than (brown) zero. Gradient of colors show range of values greater than 75% certain.

Bjorkman 1980), the water demand of the atmosphere (Day 2000), and the increased costs of respiration at higher temperatures (Sprugel et al. 1995). Alternatively,  $\beta_{\text{PRECIP}}$  will be influenced by a range of factors depending on the climatology of a region—from interannual variations in snowpack, water-supply-driven hydrologic stress, and light limitation from thick cloud cover during relatively high rainfall years. Based on the sign of  $\beta_{\text{TEMP}}$  and  $\beta_{\text{PRECIP}}$  we quantify where transitions occur between different ecological–climate interactions, suggesting how the growing season, the balance between the water demand of the atmosphere, water supply from precipitation, and the effects of clouds on solar radiation can each play a role in determining the ecosystem function in different climates. We expect ecosystem function to be determined by a myriad of time scales, so that processes that operate at a subannual scale but offset other processes will be less visible in our analysis. This is a possible explanation for the number of bins in the hot wet climates with high uncertainty, where less seasonality provides less structure for leaf drop and flushing. We note that both the analysis of the patterns of weak  $\beta_{\text{PRECIP}}$  and the uncertainty in both  $\beta_{\text{TEMP}}$  and  $\beta_{\text{PRECIP}}$  suggest that there could be offsetting or less coherent processes operating in these climates. Future investigation into the seasonal structure of  $\beta$  may help differentiate processes in areas of uncertainty.

#### b. Uncertainty

To quantify the uncertainty in the aggregate bins of  $\beta_{\text{TEMP}}$  and  $\beta_{\text{PRECIP}}$  we use a Monte Carlo technique on both the regression and the binning process, randomly choosing half the points (i.e., half the years for regression and half the points in a bin for averaging) and running the calculation 10 000 different times. This creates a regression robust to outliers and characterizes the uncertainty for  $\beta$  in time and climate space (Fig. 3). Our approach is similar to the concept of bootstrapping a

distribution for uncertainty determination (Efron 1979). Additionally, we completed our analysis with alternative datasets and found that the results are robust to the choice of dataset for both climate, using the CRU TS3.21 gridded dataset (precipitation and temperature; Jones and Harris 2013), and NDVI, using the MODIS NDVI product (Solano et al. 2010). We do see some differences between results using alternate datasets, primarily while using the shorter MODIS NDVI dataset. The analysis performed with MODIS NDVI has a generally stronger  $\beta$  and shows some change in sign in the warmer end of the transition zone for  $\beta_{\text{TEMP}}$ . The differences are partly due to the different time period covered by MODIS NDVI, and the overall pattern is qualitatively similar across different time periods, environmental data, and NDVI; differences are discussed further in the appendix (Fig. A1).

#### c. Environmental data

We perform the analysis on the 16-yr time series (1997–2012) of  $1^\circ \times 1^\circ$  latitude–longitude resolution observations where complete years of global observations of NDVI from the third generation index NDVI3g (Pinzon and Tucker 2014), near-surface air temperature from the 2-m ERA-Interim (Dee et al. 2011), and precipitation from the Global Precipitation Climatology Project (GPCP) (Adler et al. 2003) are concurrently available. We used the monthly surface temperature estimates from the 2-m ERA-Interim to represent the environmental temperature experienced by vegetation (Dee et al. 2011). We calculated a monthly precipitation dataset by summing daily precipitation from the GPCP  $1^\circ \times 1^\circ$  latitude–longitude resolution global dataset (Adler et al. 2003). The GPCP dataset is a combination of satellite and gauge data interpolated across the globe available at  $1^\circ \times 1^\circ$  from 1996 to 2012, with data for a complete year starting in 1997. Gridded datasets were interpolated to a common spatial grid with the MATLAB function `interp2.m`.

To calculate the regression of shortwave radiation and temperature we use shortwave downward surface radiation from the Surface Radiation Budget 3.1 (SRB 3.1) a  $1^\circ \times 1^\circ$  latitude–longitude monthly dataset (see Fig. 7) (Zhang et al. 2013). To create a radiatively based potential evapotranspiration (PET) estimate we use surface net downward shortwave radiation from Clouds and the Earth's Radiant Energy System–Synoptic Radiative Fluxes and Clouds (CERES-SYN) from 2001 to 2012 (Smith et al. 2011) [in appendix, see section b, Eq. (A1), and Fig. A2b). Additional interannual environmental data for temperature, precipitation, and PET from CRU TS3.21 were used to ascertain the robustness of the analysis to choice of environmental data (Jones and Harris 2013). Additional datasets of PET from MODIS and Global Land Data Assimilation System (GLDAS) were compared to ascertain the certainty of the  $P/PET$  estimate (Fig. A2a) (Mu et al. 2007; Feng and Fu 2013).

#### d. Remotely sensed vegetation

We chose NDVI as an observation of vegetation because of its global coverage and the availability of relatively long time series. The NDVI3g time series is an improved global NDVI dataset from the Advanced Very High Resolution Radiometer (AVHRR) (Pinzon and Tucker 2014). The dataset has a  $1/12^\circ$  latitude–longitude resolution and global coverage of 15-day global maximum composites. Processing the datasets into maximum composites reduces the effects from clouds and the satellite viewing angle (Holben 1986). To create a common time step we created monthly maximum composites from the NDVI 15-day composites before calculating an annual mean time series from 1983 to 2012. We interpolated the data to  $1^\circ$  by  $1^\circ$  spatial resolution prior to analysis and shortened the NDVI time series to 1997–2012 to match the spatial scale and temporal range of the environmental data.

In this study we will interpret NDVI as a proxy for the surface greenness and chloroplast density and use it to calculate the interannual variation of vegetation. NDVI is calculated by normalizing the difference between the visible channel and near-infrared channel from the AVHRR instruments by the sum of the channels. Vegetation absorbs strongly in the visible band, distinguishing it from soils and other nonvegetated surfaces. Though not directly used here, NDVI also relates to leaf area index and fraction of absorbed photosynthetically active radiation (Myneni et al. 2002); thus we consider the signal from NDVI as primarily related to the leaves of vegetation and their potential to fix sunlight into sugars. We assume here that the greening of an ecosystem relative to the climatological mean signals that it is advantageous for the plants to deploy more chloroplasts in an attempt to fix more carbon. On

an annual basis, we use an increase in greenness as a metric for a positive sensitivity of vegetation to climate that correlates with increased net primary production (Myneni et al. 1995).

The launch of satellites with instruments that measure additional spectral bands has allowed for the creation of new vegetation indices and remote observations of vegetation. For example, observations from the Moderate Resolution Imaging Spectroradiometer (launched in 1999) are used to generate an improved NDVI product with less interference from water vapor as well as the enhanced vegetation index (EVI), which uses a blue measurement channel to reduce the effects of aerosols (Solano et al. 2010). In general, both NDVI and EVI from MODIS have been shown to have larger seasonal amplitudes than NDVI from AVHRR, and EVI in particular does not saturate over high biomass areas as much as NDVI has been shown to (Huete et al. 2002). There is also the exciting new development of solar-induced fluorescence as a more direct observation of the photosynthetic activity, and thus gross primary productivity (GPP) (Frankenberg et al. 2014). Though NDVI has been shown to relate to GPP, it is not completely proportional and can show markedly different relationships between different vegetation types (Frankenberg et al. 2011; Guanter et al. 2012). Exploration of the measurement of solar-induced fluorescence is just getting under way using observations from *Greenhouse Gases Observing Satellite* (GOSAT) and *Orbiting Carbon Observatory 2* (OCO-2) and do not yet have long enough time series to investigate the interannual ecological–climate interactions.

#### e. Standardization

We chose to standardize the NDVI time series in order to show the magnitude of the interannual change compared to the average NDVI of the pixel [Eq. (2)]:

$$\% \Delta_{\text{NDVI}} = \frac{(\text{NDVI} - \overline{\text{NDVI}})}{\overline{\text{NDVI}}}, \quad (2)$$

where  $\% \Delta_{\text{NDVI}}$  is the interannual percent change of NDVI, NDVI is the full time series (1983–2012), and  $\overline{\text{NDVI}}$  is the average of the full time series (1983–2012). We chose not to alter the predictor variables of temperature and precipitation so that our analysis produced a metric that is consistent across the globe ( $\% ^\circ\text{C}^{-1}$  or  $\% \text{mm}^{-1}$ ), rather than being standardized by a local effect (e.g., by environmental mean or interannual standard deviation).

#### f. Removing nonvegetated terrestrial grid points

Our analysis considers only vegetated terrestrial grid points by removing ocean and nonvegetated land grid



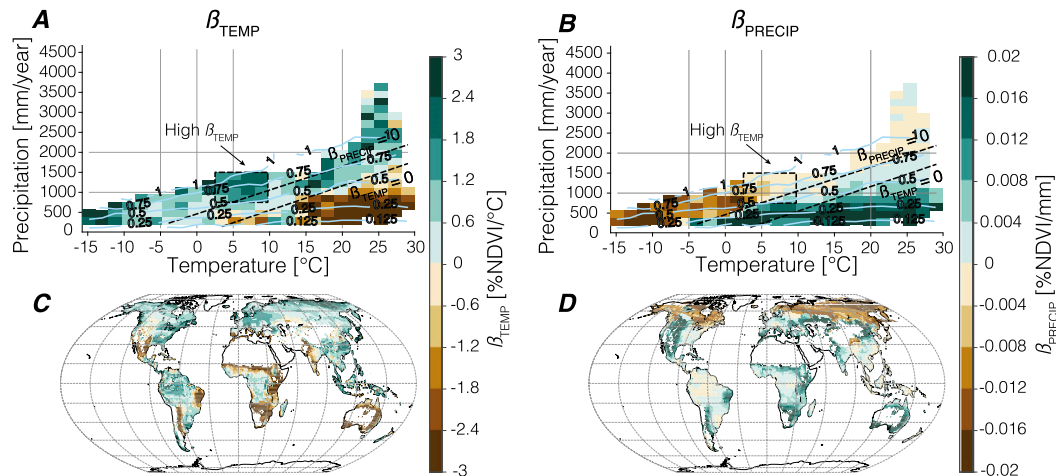


FIG. 4. Sensitivity of vegetation to interannual variation from 1997–2012 in (a) temperature  $\beta_{TEMP}$  and (b) precipitation  $\beta_{PRECIP}$ . Each pixel displayed is the average value of all spatial points found in locations with particular climatological mean annual temperature and mean annual precipitation. Shades of green (brown) show positive (negative) sensitivity [greener vegetation when (a) warmer (cooler) or (b) wetter (drier)]. Blue contours in (a) and (b) are of  $P/PET$  derived from precipitation and shortwave radiation. The thick dashed black line marks the transition in sensitivity ( $\beta_{TEMP} = 0$ ;  $\beta_{PRECIP} = 0$ ). Boxes in (a) and (b) mark areas of particularly high  $\beta_{TEMP}$ . Light gray lines are for reference. A map of the average (c)  $\beta_{TEMP}$  and (d)  $\beta_{PRECIP}$  from each climate bin [as shown in (a) and (b)] is shown reprojected onto a spatial map.

points (Fig. 1). We removed ocean grid points using the water mask included in the NDVI3g data files. We determined a grid point to have a nonvegetated year when the three months with maximum NDVI values either had a minimum monthly value less than 0.1 or a mean of the three months that was less than 0.3, as adapted from Zhou et al. (2001) (Fig. 1). If a pixel was nonvegetated in any of the 30 years between 1983 and 2012 it was removed from further analysis. This filtering results in the removal of 3726 points of the possible 14 693 land points (25%) and can be visualized in Fig. 2. Defining vegetated points in this way likely removes some points that are vegetated at some point during the time series. For example, removing points with vegetation recovering from bare ground (e.g., afforestation) or where vegetation has been removed to bare ground (e.g., deforestation, fire). Removing nonvegetated grid points with this threshold also removes particularly low NDVI. This removes the danger of dividing by zero in the standardization and creating falsely high sensitivity with no real ecological significance.

### 3. Results and discussion

#### a. Broad pattern of $\beta_{TEMP}$ and $\beta_{PRECIP}$

Aggregated  $\beta_{TEMP}$  and  $\beta_{PRECIP}$  vary systematically across global climate gradients (Figs. 4a,b). Large values of  $\beta$  highlight areas where ecosystem greenness

generally responds strongly, and predictably, to interannual changes in the climate (temperature or precipitation in this study), without being limited by other resources required for greenness. The pattern of  $\beta_{TEMP}$  and  $\beta_{PRECIP}$  bin aggregated in the climate space of mean annual temperature and mean annual precipitation explains a large portion of the pixel-by-pixel global variation of  $\beta_{TEMP}$  (26%) and  $\beta_{PRECIP}$  (37%) (Figs. 4a,b). Considering the diversity of factors influencing the sensitivity of vegetation greenness to climate, the substantial amount of variance explained by the annual climate of temperature and precipitation suggest mean annual temperature and mean annual precipitation are strong controls on ecosystem function. The systematic variations of ecosystem functioning across mean annual temperature and precipitation supports why these climate variables have traditionally been included in biogeographic explanations of biomes. The remaining unexplained variance in  $\beta_{TEMP}$  and  $\beta_{PRECIP}$  may be due to other climate variables (e.g., solar radiation or the climate seasonality), local controls (such as soil structure or successional history), unidentified stochastic processes (such as storm damage or multiyear effects of fire), strong gradients not represented by the coarse aggregation, or measurement noise.

We observe inflections between positive and negative  $\beta_{TEMP}$  and  $\beta_{PRECIP}$  extending as lines across a large range of average climates (Figs. 4a,b). The linearity of the inflection lines suggest that ecosystem performance near

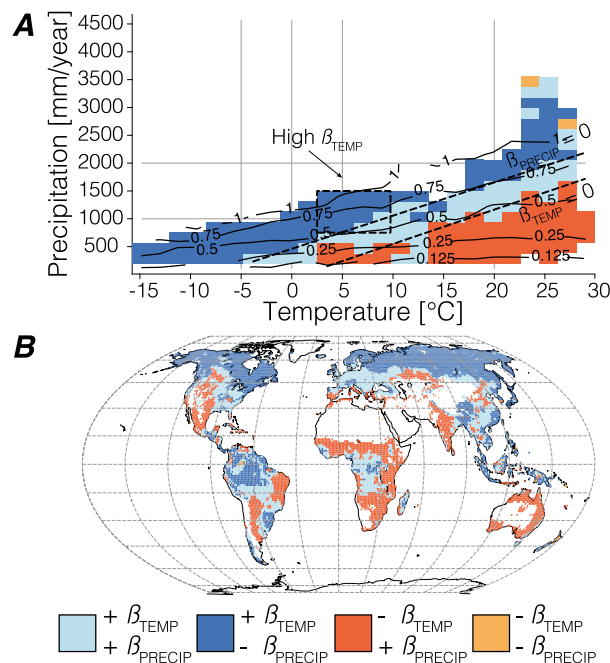


FIG. 5. Comparison of the sign of  $\beta_{TEMP}$  and  $\beta_{PRECIP}$  is shown in (a) climatological mean annual temperature and mean annual precipitation space and (b) projected onto a spatial map. Pixels are colored light blue where both  $\beta_{TEMP}$  and  $\beta_{PRECIP}$  are positive (warmer, wetter, greener), dark blue where  $\beta_{TEMP}$  is positive but  $\beta_{PRECIP}$  negative (warmer, drier, greener), dark orange where  $\beta_{TEMP}$  negative and  $\beta_{PRECIP}$  positive (colder, wetter, greener), and light orange where both negative (colder, drier, greener). Light gray lines in (a) are as described in Fig. 4 and black contours of  $P/PET$ .

$\beta = 0$  is determined by the proportional amount of average precipitation relative to the average temperature of a location. It is notable that both of the inflection lines ( $\beta_{TEMP}$  or  $\beta_{PRECIP} = 0$ ) are approximately parallel (slope of 62.5 to 59 mm yr<sup>-1</sup> °C<sup>-1</sup>), as they highlight different aspects of ecosystem functioning, but offset by 7.9°C (mean annual temperature intercept of 1.1°C for  $\beta_{TEMP}$  and -6.8°C for  $\beta_{PRECIP}$ ) (Figs. 4a,b). Near the inflection line, the ecosystem performance is dependent on both the average temperature and precipitation of a region. Thus there is equivalence between temperature and precipitation such that the performance cost of moving to a 1.7°C warmer climate region can be offset by an additional 100 mm yr<sup>-1</sup> of rainfall.

We hypothesize that the proportional relationship between  $T$  and  $P$  is operating through the water balance of the vegetation. The evidence for the relation of the proportionality of  $T$  and  $P$  to water balance comes from three arguments: dependence of atmospheric water demand being a function of temperature, the presence of the proportionality across multiple datasets (see appendix), and the presence of the mechanism in previous

work on plant hydraulics (McDowell 2011; Grier and Running 1977). As temperature increases, the temperature-driven increase in atmospheric demand for water increases PET, causing hydrologic stress. Hydrologic stress can then be offset for plants if more water is supplied through precipitation. Other aspects of the environment that we do not account for have the potential to exacerbate the annual imbalance (seasonality of water demand and supply leading to runoff) and soil water storage (helping balance offset of supply and demand) and matric water potential of soils (resisting vegetation in meeting the atmospheric demand) (Borchert 1994). With these additional mechanisms in consideration it is notable that though the proportional relationship between  $T$  and  $P$  spans a large range of climates, it is only observed as a proportional in a relatively narrow transition zone. A similarly sloped line between the max correlation of temperature and precipitation with gross primary productivity derived from flux towers is evident (but not discussed) in a paper from Jung et al. (2011, their Figs. 8c,f). Physiological experiments also provide evidence of temperature influencing plants through atmospheric water demand. When the direct effects of temperature increases on vegetation are isolated from the temperature-driven increase in vapor pressure deficit, the vapor pressure effects are large relative to the direct temperature effects at warmer temperatures (Day 2000). From this we expect increases in atmospheric water demand, in the form of vapor pressure deficit, to be the dominant constraint on vegetation in places with relatively warm temperatures (above 16°C).

These observations of proportionality between temperature and precipitation also qualitatively agree with arguments that aridity (precipitation divided by potential evapotranspiration  $P/PET$ ) is a critical climate variable in shaping ecosystems (e.g., Budyko 1961; Lugo et al. 1999). However, though contours of  $P/PET$  plotted across mean annual temperature and precipitation share the sign of the inflection contours, they have a slope ( $\approx 30$  mm yr<sup>-1</sup> °C<sup>-1</sup>) that is consistently half that of the inflection lines that we observe (Figs. 4a,b and 5a). This consistent line of transition and mismatch with  $P/PET$  is evidence either that vegetation has access to a consistent fraction of precipitation, less than the total precipitation, across a wide range of climates or that vegetation is more sensitive to changes in potential evapotranspiration than can be explained by  $P/PET$ . The consistency of the trade-off between temperature and precipitation for both  $\beta_{PRECIP}$  and  $\beta_{TEMP}$  suggests a fundamental relationship between plant physiology and climate. The broad climate range (-5° to 28°C and mean annual precipitation of 200 to 2000 mm yr<sup>-1</sup>) across which the

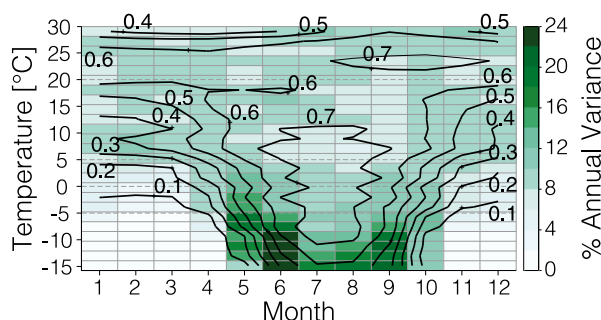


FIG. 6. The variance for each month in NDVI divided by the annual sum of monthly variance, shown across a range of annual mean temperatures in the Northern Hemisphere. Months with higher percent variance (dark green colors) contribute more strongly to the annual mean variance. Contours show mean monthly NDVI values.

lines of inflection extend suggest that there is a strong ability for ecosystems to adapt to their climate and account for the negative effects of increased PET (driven by temperature) with increases in net photosynthesis due to increased temperature (Berry and Bjorkman 1980). We find that the lower slope of  $P/PET$  isopleths compared to those of  $\beta_{TEMP}$  and  $\beta_{PRECIP}$  is robust across multiple datasets of potential evapotranspiration, though the magnitudes of the pixel-by-pixel  $P/PET$  values are uncertain owing to a wide spread between datasets on the values of PET (see methods and Fig. A2a).

In the following sections we further discuss hypotheses for the mechanisms governing the climate–vegetation interactions consistent with the observed pattern of  $\beta_{TEMP}$  and  $\beta_{PRECIP}$ , particularly in regard to the combination of their signs. We discuss regions where growing season length, water, and solar insolation limit greenness.

#### b. Growing season limited: Temperature and snow cover

Vegetation is greener during both warmer and drier years in the coldest, driest vegetated areas of the globe, as well as places with annual mean temperatures up to relatively warm values of 15°C where precipitation is also high (1500 mm yr<sup>−1</sup>) (Fig. 5a). Places with these climates are primarily spatially located at high latitudes and experience a large seasonality in temperature and sunlight. These climate conditions lead to a growing season duration constrained by low temperatures and late snow cover melt (Takala et al. 2011) (Figs. 4c,d and 5b). We hypothesize that the main driver of variability on annual greenness is the duration of the growing season. Thus, we expect to see this mechanism acting mainly in the months at either end of the growing season

rather than during months of peak greenness. In addition, these months are favored by atmospheric patterns of blocking and ENSO variation that might suggest that the climate in these months is also critical to setting the length of the growing season (Lejenäs and Økland 1983). Indeed, the months with the most variance in NDVI in cold (<−5°C) Northern Hemisphere locations are June (beginning of growing season) and September (end of growing season) (Fig. 6). In places with a mean annual temperature below −5°C there is very limited variance of NDVI during winter (November to April), including places with mean annual temperatures below −10°C where the variance drops to zero in winter (Fig. 6). Months with proportionally more variance in NDVI will most strongly influence the interannual NDVI variance. Therefore, for these very cold regions (<−5°C) the shoulder months of the growing season primarily determine whether a year is greener or browner.

We hypothesize that the mechanism limiting vegetation greenness in these areas characterized by cold temperatures with both positive  $\beta_{TEMP}$  and negative  $\beta_{PRECIP}$  is a combination of temperature and snow; years with warmer average temperatures or drier years with less snow correspond to greener years. Warmer temperatures and an earlier snowmelt are likely to correspond to more days during which conditions are favorable for growth. This mechanism is consistent with the hypothesis that the effects of the interannual variation in temperature and precipitation occur primarily in the shoulder months. In warmer climates the variance of NDVI becomes less concentrated in the shoulder months, and in places with an average temperature above 5°C, the variance is more evenly spread across all months (Fig. 6).

#### c. Water limited: Hot and dry

Nearly all of the negative values of  $\beta_{TEMP}$  (greener in cooler years) occur in places with mean annual temperatures above 15°C and precipitation less than 1000 mm yr<sup>−1</sup> (Fig. 5a). The relatively large positive values of  $\beta_{PRECIP}$  suggest that greenness in drier years is driven by hydrologic stress from limited water supply. The combination of general greening during either cooler or wetter years shows that hydrologic stress is driven by both the supply of water and the atmospheric demand for water as discussed above.

Locations falling in the hot dry region are primarily clustered along the edges of nonvegetated deserts of the North American Southwest, the Sahel, South Africa, and Australia as well as northeast Brazil and the rain shadow of the Chilean coastal range (Figs. 4c and 5d). Nonvegetated points in deserts have been explicitly



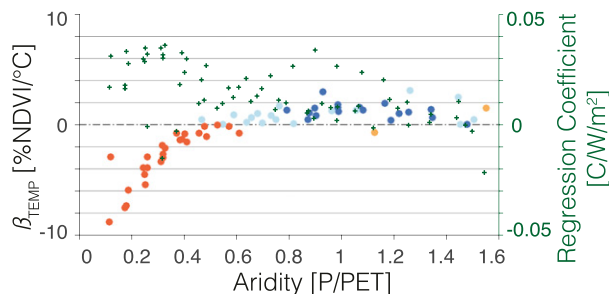


FIG. 7. Variation of  $\beta_{\text{TEMP}}$  (filled circles, colors as in Fig. 5; left axis) and regression coefficient of interannual temperature and shortwave radiation (green crosses; higher values show strong positive coupling between temperature and shortwave radiation; right axis) across places with different mean annual PET for locations with mean annual temperature greater than 20°C.

eliminated from this analysis, but plants living in these places are presumably limited by water availability as well. Because of the extensive spatial extent of the hot dry region and deserts we hypothesize that low precipitation is the most common limitation on global vegetation. In climate regions with 0.2 to 0.5  $P/PET$ ,  $\beta_{\text{TEMP}}$  and  $\beta_{\text{PRECIP}}$  both weaken rapidly as the increased water supply relieves the hydrologic stress from the temperature-driven increase in atmospheric water demand (Figs. 4a,b). As the climate becomes wetter, the signs of both  $\beta_{\text{TEMP}}$  and  $\beta_{\text{PRECIP}}$  change, becoming positive (greener when warmer) and negative (greener when drier), respectively. The certainty of  $\beta_{\text{PRECIP}}$  becomes limited in the hottest, wettest regions of the globe, while  $\beta_{\text{TEMP}}$  has stronger certainty (Fig. 3).

#### d. Energy limited: Interaction of clouds and sunlight

Areas with positive  $\beta_{\text{TEMP}}$  and negative  $\beta_{\text{PRECIP}}$  occur where rainfall is above 2000 mm yr<sup>-1</sup> and temperatures are above 20°C; these areas include most of the Amazon basin and the Maritime Continent (Fig. 5). To be generally greener during warmer years at these high temperatures, we hypothesize that plants must offset high respiration costs associated with warmer years with even larger increases in productivity (Fig. 4a). To complicate matters, net photosynthesis measured experimentally at the plant scale shows a decrease at high temperatures, with a limit commonly seen around 30°C, and this holds true even for those plant species adapted to high temperatures (optimum at 46°C) (Berry and Bjorkman 1980; Day 2000).

One pathway that could explain generally increased greenness in warm years for these locations is for light limitation on photosynthesis to be relieved by additional insolation. Along a gradient of increasing  $P/PET$ ,  $\beta_{\text{TEMP}}$  begins strongly negative (brownier when warmer) at low

$P/PET$  but increases rapidly as  $P/PET$  increases in this relatively arid climate region (less than about 0.5) (Fig. 7). The  $\beta_{\text{TEMP}}$  transitions to positive values between  $P/PET$  values of 0.5 and 0.8 and then is generally positive along with a positive  $\beta_{\text{PRECIP}}$  above 0.8. Budyko (1961) hypothesized that a transition in the surface balance of water demand and water supply occurs from water-limited evaporation conditions (more potential evapotranspiration than water available) to energy limited (more water available than insolation) as water availability increases. The shape of these observations is indicative of  $\beta$  responding to regions of water limitation ( $< 0.5$ ) and energy limitation ( $> 0.8$ ).

We also note that interannual increases in temperature are concomitant with greater increases in insolation in wetter climate regions (sunnier, less clouds when warmer) (Fig. 7). We observe approximately a factor-of-2 change in the concomitant change of insolation with temperature ( $\text{W m}^{-2} \text{ } ^\circ\text{C}^{-1}$ ) between  $P/PET$  values of 0.2 and 0.8 (Fig. 7). Increased water availability changes the relationship of sunlight and temperature, diverting more of the surface energy flux through latent heat rather than sensible heat. Thus, the same increase in photosynthetically active radiation does not lead to the same increase in air temperature as in drier regions. With a positive  $\beta_{\text{TEMP}}$  and negative  $\beta_{\text{PRECIP}}$  it is apparent that any hydrologic stress from the increase in water demand by a warmer atmosphere is being offset by ample water supply and concurrent increases in solar radiation, allowing for enhanced vegetation greenness during warmer years even at these high temperatures (Fig. 7).

The response of ecosystem function in hot, wet regions to a changing climate may have strong implications for the terrestrial carbon cycle feedback on climate change. These hot, wet climate regions tend to have very large pools of aboveground carbon storage (Simard et al. 2011; Saatchi et al. 2011) and encompass the tropical rain forests in South America, Africa, and Indonesia, as well as southeast China (Figs. 4c,d and 5b). Our results suggest that concomitant increases in shortwave radiation act as a mediator on the effect of warming on greening in these hot, wet regions. We hypothesize that these ecosystems would have a different sensitivity to warming if it occurred without increases in solar radiation (i.e., from greenhouse gasses). Ecosystems would also likely have different sensitivity to a multiyear decline in rainfall such as from an extended drought as opposed to interannual variability. These long-term changes would instead drive the whole ecosystem down the precipitation gradient out of the hot, wet region toward positive  $\beta_{\text{PRECIP}}$  below 2000 mm yr<sup>-1</sup> (Figs. 4c,d).

### *e. Climate change implications*

Observations of  $\beta$  derived from greenness suggest that ecosystem functioning depends on multiple physical aspects of climate, as well as the coordinated changes among them. Predicting the future changes of some of aspects of climate is much more difficult (i.e., rainfall), which helps explain the uncertainty in current predictions of the carbon cycle (Friedlingstein et al. 2006). In addition, climate change may not maintain the same concomitant changes that we can observe in interannual climate variations (e.g., temperature's damped response to sunlight in wetter climates). Predictions based on any one variable alone (e.g., temperature) will not do as well where these concomitant changes are strong drivers, with ramifications for predictions ranging from global climate sensitivity to food supply (Friedlingstein et al. 2006; Battisti and Naylor 2009). In particular, temperature is likely to increase as a result of greenhouse gasses without an associated change in shortwave radiation. The strong implied effects of covariation of temperature with shortwave radiation should motivate future research to investigate the interconnections between climate variables under climate change and take into account their location in climate space.

To aid in predictions of new climate regimes our empirical characterization of present-day relationships between ecosystem functioning and climate can also serve as an observationally based constraints to improve process-based models (Luo et al. 2012). Comparing our linear metrics of the sensitivity of vegetation to climate with model output probes the veracity of ecosystem-climate interactions directly rather than the final results of these interactions (e.g., sensitivity of vegetation to temperature, rather than solely the temperature or greenness of a particular region). This added constraint complements and could possibly enhance other efforts to improve the representation of processes within global vegetation models. These observational constraints will improve simulations not only under current conditions but also under novel conditions by improving the functional fidelity of the global vegetation model. Improved models can then make better predictions despite the differences between present-day observed variability and anthropogenic-driven global warming of the next century.

**Acknowledgments.** We would like to acknowledge Leander Love-Anderegg, Robin Ross, Langdon Quetin, Marysa Lague, Elizabeth Garcia, and Marlies Kovenock for providing comments on the paper. The work was partially conducted while GRQ was supported by the

University of Washington Program on Climate Change Fellowship. We would also like to acknowledge the Keck Institute for Space Studies at the California Institute of Technology who hosted GRQ during part of this work. We acknowledge National Science Foundation Grants AGS-1321745 and AGS-1553715.

All the original data used in our analysis are listed in the references.

## APPENDIX

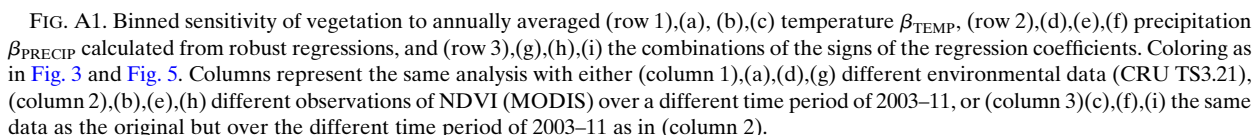
### **Uncertainty Analysis in Linear Regression, Binning, and Datasets**

To establish the uncertainty and robustness of the analysis of ecological climate interaction across climate space we performed four experiments: a Monte Carlo bootstrap uncertainty estimate (section a), an experiment using the shorter time series available from MODIS NDVI (section b), an experiment with the CRU TS3.21 dataset representing statistically upscaled station observations of the environment (section c), and an experiment omitting grid points with strong interannual correlation between precipitation and temperature (section d) (Figs. 3 and A1). Results generally show low uncertainty in the sign of  $\beta$  outside of the transition area and the hot, wet region, and they are qualitatively consistent using MODIS NDVI and CRU TS3.21 in place of NDVI3g and the combination of ERA-Interim and GPCP, as well as when points of high correlation are omitted. Methodology and specific differences are discussed below.

#### *a. Estimating uncertainty of $\beta$ in time and climate space*

To estimate the uncertainty in the regression coefficient values  $\beta$ , we used a bootstrap Monte Carlo technique, similar to method 2 discussed in Efron (1979), in combination with the regression at each grid point (Fig. 1). We performed 10 000 regressions by randomly drawing 8-yr time series from the total 16-yr dataset. The mean of these 10 000  $\beta$  values is reported as the sensitivity of vegetation (Fig. 4). The resulting distributions of sensitivity are combined with the uncertainties from the bins to determine 95% bounds on the uncertainty (Fig. 3).

To aggregate patterns of the  $\beta$  across climate space, each geospatial point was assigned a bin dictated by its climatological mean annual temperature and precipitation. There are 178 bins, each 1.8°C by 186.5 mm yr<sup>-1</sup>; bins with fewer than 10 points were ignored (Figs. 2 and 1a,b). We include all 10 000 vegetation sensitivities



The uncertainty analysis includes the contributions of both the uncertainty in the regression (i.e., the consistency of the ecological climate interaction across time) and the uncertainty in each bin (i.e., the consistency in the ecological–climate interaction in any particular climate bin). The uncertainty in sign for  $\beta_{\text{TEMP}}$  is strongest in the hot, wet climates and along the sloping transitions

from positive  $\beta_{\text{TEMP}}$  to negative  $\beta_{\text{TEMP}}$ . In comparison, the uncertainty in  $\beta_{\text{PRECIP}}$  also shows the sloping transition line and is particularly low for climate regions below precipitation values of  $1500 \text{ mm yr}^{-1}$ . Again, the hot, wet climate regions are particularly uncertain. The aggregated patterns of uncertainty show similar patterns to those of the mean  $\beta$  values, suggesting that the consistency of  $\beta$  generally follows the strength of  $\beta$ . This uncertainty appears to be a function of climate as well. The differences in the analysis due to using different vegetation indices and environmental datasets also primarily occur in regions where the temporal and binning uncertainty are highest. This correlation is to be expected if the patterns of the analysis done with different datasets are approximately the same as the original analysis, as the sign and amplitude are more likely to change where the analysis was uncertain in the first place.

#### *b. Analysis with MODIS NDVI*

As noted above there are multiple other remotely sensed vegetation indices, as well as multiple corrections to the NDVI vegetation index (Hilker et al. 2014; Solano et al. 2010; Holben 1986). To test the robustness of the observed patterns to our choice in NDVI product, we compared the newer MODIS NDVI observations that are available from 2003 to 2015 with the overlapping portion (2003–11) of NDVI3g with complete years. Qualitatively these analyses are very similar to those of the original analysis using NDVI3g from 1997 to 2012 (Fig. A1, right two columns). Hot, dry climates have negative  $\beta_{\text{TEMP}}$  and positive  $\beta_{\text{PRECIP}}$  (greening when cooler and wetter), and the cold regions show positive  $\beta_{\text{TEMP}}$  and negative  $\beta_{\text{PRECIP}}$  (greening when warmer and drier); there is evidence of the sloped optimums ( $\beta = 0$ ), and the hot, wet climates show a mix of both  $\beta_{\text{TEMP}}$  and  $\beta_{\text{PRECIP}}$  but are predominantly greener when warmer and drier. We observe a few notable differences. First, the MODIS NDVI results have generally stronger sensitivities (Figs. A1b,e). This result follows from the observations that the seasonal cycle of MODIS NDVI is stronger than that of NDVI3g, which would lead us to expect that the interannual variation would also be stronger (Huete et al. 2002). Second, the cold region shows many more points where there is a greening during wetter years (Figs. A1b,e). However, the location of the change from generally negative  $\beta_{\text{PRECIP}}$  to positive  $\beta_{\text{PRECIP}}$  is preserved, particularly in drier climates. This is not entirely the case for  $\beta_{\text{TEMP}}$ ; at lower rain levels there is a clear transition zone, but at the wetter/warmer end of this transition zone the region of greening when cooler has expanded. It is not completely unexpected that there would be instability in this region, as

it is the least certain in our original analysis, and the 2003–11 time window shows some encroachment of greener when cooler and wetter even in the shortened NDVI3g analysis (Figs. 4a,b and Figs. A1c,f,i; cf. second and third columns).

#### *c. Analysis with other environmental data*

To ascertain the robustness of the analysis to choice of environmental datasets we used alternate environmental data from CRU TS3.21. We performed the regressions over the same time period 1997–2012 with CRU TS3.21 temperature and precipitation and NDVI3g vegetation index (Figs. A1a,d,g). CRU TS3.21 was chosen because it uses a different method to derive global gridded datasets of temperature and precipitation. Rather than a reanalysis product (such as ERA-Interim) or a combination of gauge and remote sensing observations (such as GPCP), CRU TS3.21 is a statistically upscaled gridded product based on station data. Station coverage is relatively dense over North America and Europe and particularly sparse over tropical South America and Africa. Our results using CRU TS3.21 show that the analysis using a different environmental dataset is qualitatively similar and continues to support our results and discussion (cf. Figs. 4a,b and 5a with Figs. A1a,d,g).

#### *d. Temperature and precipitation correlation*

The predictor variables of interannual temperature and precipitation used in the linear regression are often collinear in nature. Where there is particularly strong correlation, there is the possibility that a multilinear regression will not do a good job of separating the variation explained by each predictor variable. To address this concern we ran a test by omitting points from our analysis that have higher correlation coefficients ( $>0.6$  correlation). We find nearly no change to our analysis and no changes to our overall interpretation and discussion of the results. We determine that pixels with high correlations between temperature and precipitation do not appear to have undue influence on the aggregated pattern discussed in the manuscript.

Our omission of pixels with correlations above 0.6 (36% shared variance) is conservative per the statistical literature where it is suggested that correlation coefficients of up to 0.77 (60% shared variance) can be linearly separated and even some suggestion that values as high as a correlation coefficient of 0.89 (80% shared variance) are acceptable (O'Brien 2007). Only a small portion of the global area analyzed exceeds a correlation coefficient between precipitation and temperature of 0.6.



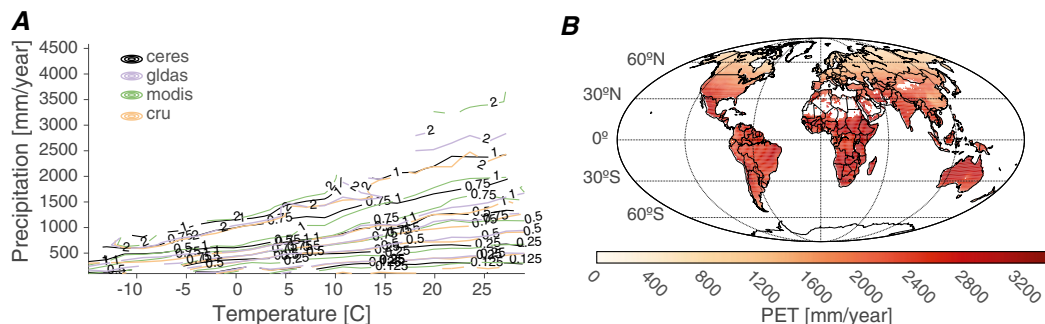


FIG. A2. (a) Contours of binned long-term means of multiple datasets of potential evapotranspiration. Binned values are contoured at values as in the Holdridge life zones chart and displayed in temperature and precipitation climate space. (b) map of mean PET from 2001 to 2012 created from CERES-SYN net shortwave downward surface radiation. Colors are in  $\text{mm yr}^{-1}$  of potential evapotranspiration.

### e. Variability across aridity datasets

Vegetation health and productivity is driven by a balance of the supply and demand of water in many environments. Aridity is a measurement of the dryness of an environment that takes both the supply of water (precipitation  $P$ ) and the demand for water [potential evapotranspiration (PET)] into account. Potential evapotranspiration can be calculated in a number of ways based on net radiation [Eq. (2)] (Budyko 1961), empirical temperature-based relationships (CRU TS3.21), and a more complete Penman–Monteith approach that treats the complete surface energy budget (MODIS PET and GLDAS PET) (Smith et al. 2011; Jones and Harris 2013; Mu et al. 2007; Feng and Fu 2013). We investigated a number of observationally derived products of PET to use in combination with precipitation from GPCP to create an aridity index of  $P/\text{PET}$ . We found that the absolute values of aridity ( $P/\text{PET}$ ) were highly variable, owing to different estimates of PET, but that the slopes of the contours binned across precipitation and temperature were relatively stable (Fig. A2a). From this we conclude that our comparisons of the slope of the optimal lines ( $\beta = 0$ ) with contours of  $P/\text{PET}$  are robust but that the actual values of  $P/\text{PET}$  at which changes in ecological–climate interaction change are unknown owing to uncertain global estimates of PET (Fig. 7). For our comparison we chose the simplest of the PET estimates that depends only on the net downward shortwave radiation (Budyko 1961). Using observations from CERES-SYN, we calculated PET in order to calculate  $P/\text{PET}$  to compare with  $\beta$  (Fig. A2b):

$$\text{PET} = \frac{S_w}{L_v \rho_w} \quad (\text{A1})$$

PET is calculated as the amount of water that the energy available in the net downward shortwave radiation  $S_w$

could possibly evaporate by dividing it by the latent heat of vapor  $L_v$  and the density of water  $\rho_w$ .

### REFERENCES

- Adler, R. F., and Coauthors, 2003: The Version-2 Global Precipitation Climatology Project (GPCP) monthly precipitation analysis (1979–present). *J. Hydrometeorol.*, **4**, 1147–1167, doi:10.1175/1525-7541(2003)004<1147:TVGPCP>2.0.CO;2.
- Asner, G. P., A. R. Townsend, and B. H. Braswell, 2000: Satellite observation of El Niño effects on Amazon forest phenology and productivity. *Geophys. Res. Lett.*, **27**, 981–984, doi:10.1029/1999GL011113.
- Baldocchi, D., 2014: Measuring fluxes of trace gases and energy between ecosystems and the atmosphere—The state and future of the eddy covariance method. *Global Change Biol.*, **20**, 3600–3609, doi:10.1111/gcb.12649.
- Battisti, D. S., and R. L. Naylor, 2009: Historical warnings of future food insecurity with unprecedented seasonal heat. *Science*, **323**, 240–244, doi:10.1126/science.1164363.
- Beer, C., and Coauthors, 2010: Terrestrial gross carbon dioxide uptake: Global distribution and covariation with climate. *Science*, **329**, 834–838, doi:10.1126/science.1184984.
- Berry, J., and O. Björkman, 1980: Photosynthetic response and adaptation to temperature in higher plants. *Annu. Rev. Plant Physiol.*, **31**, 491–543, doi:10.1146/annurev.pp.31.060180.002423.
- Boisvenue, C., and S. W. Running, 2006: Impacts of climate change on natural forest productivity evidence since the middle of the 20th century. *Global Change Biol.*, **12**, 862–882, doi:10.1111/j.1365-2486.2006.01134.x.
- Borchert, R., 1994: Soil and stem water storage determine phenology and distribution of tropical dry forest trees. *Ecology*, **75**, 1437–1449, doi:10.2307/1937467.
- Budyko, M. I., 1961: The heat balance of the Earth's surface. *Sov. Geogr.*, **2**, 3–13, doi:10.1080/00385417.1961.10770761.
- Chen, B., and Coauthors, 2014: Changes in vegetation photosynthetic activity trends across the Asia–Pacific region over the last three decades. *Remote Sens. Environ.*, **144**, 28–41, doi:10.1016/j.rse.2013.12.018.
- Churkina, G., and S. W. Running, 1998: Contrasting climatic controls on the estimated productivity of global terrestrial biomes. *Ecosystems*, **1**, 206–215, doi:10.1007/s100219900016.
- Day, M. E., 2000: Influence of temperature and leaf-to-air vapor pressure deficit on net photosynthesis and stomatal

- conductance in red spruce (*Picea rubens*). *Tree Physiol.*, **20**, 57–63, doi:[10.1093/treephys/20.1.57](https://doi.org/10.1093/treephys/20.1.57).
- Dee, D. P., and Coauthors, 2011: The ERA-Interim reanalysis: Configuration and performance of the data assimilation system. *Quart. J. Roy. Meteor. Soc.*, **137**, 553–597, doi:[10.1002/qj.828](https://doi.org/10.1002/qj.828).
- Efron, B., 1979: Bootstrap methods: Another look at the jackknife. *Ann. Stat.*, **7**, 1–26, doi:[10.1214/aos/1176344552](https://doi.org/10.1214/aos/1176344552).
- Feng, S., and Q. Fu, 2013: Expansion of global drylands under a warming climate. *Atmos. Chem. Phys.*, **13**, 10 081–10 094, doi:[10.5194/acp-13-10081-2013](https://doi.org/10.5194/acp-13-10081-2013).
- Frankenberg, C., and Coauthors, 2011: New global observations of the terrestrial carbon cycle from GOSAT: Patterns of plant fluorescence with gross primary productivity. *Geophys. Res. Lett.*, **38**, doi:[10.1029/2011GL048738](https://doi.org/10.1029/2011GL048738).
- , J. Berry, L. Guanter, and J. Joiner, 2013: Remote sensing of terrestrial chlorophyll fluorescence from space. SPIE Newsroom, doi:[10.1117/2.1201302.004725](https://doi.org/10.1117/2.1201302.004725).
- , C. O'Dell, J. Berry, L. Guanter, J. Joiner, P. Khler, R. Pollock, and T. E. Taylor, 2014: Prospects for chlorophyll fluorescence remote sensing from the Orbiting Carbon Observatory-2. *Remote Sens. Environ.*, **147**, 1–12, doi:[10.1016/j.rse.2014.02.007](https://doi.org/10.1016/j.rse.2014.02.007).
- Friedlingstein, P., and Coauthors, 2006: Climate–carbon cycle feedback analysis: Results from the C<sup>4</sup>MIP model intercomparison. *J. Climate*, **19**, 3337–3353, doi:[10.1175/JCLI3800.1](https://doi.org/10.1175/JCLI3800.1).
- Ghimire, B., C. A. Williams, J. Masek, F. Gao, Z. Wang, C. Schaaf, and T. He, 2014: Global albedo change and radiative cooling from anthropogenic land-cover change, 1700 to 2005 based on MODIS, land-use harmonization, radiative kernels, and reanalysis. *Geophys. Res. Lett.*, **41**, 9087–9096, doi:[10.1002/2014GL061671](https://doi.org/10.1002/2014GL061671).
- Glenn, P. E., R. A. Huete, L. P. Nagler, and G. S. Nelson, 2008: Relationship between remotely-sensed vegetation indices, canopy attributes and plant physiological processes: What vegetation indices can and cannot tell us about the landscape. *Sensors*, **8**, 2136–2160, doi:[10.3390/s8042136](https://doi.org/10.3390/s8042136).
- Goward, S. N., B. Markham, D. G. Dye, W. Dulaney, and J. Yang, 1991: Normalized difference vegetation index measurements from the advanced very high resolution radiometer. *Remote Sens. Environ.*, **35**, 257–277, doi:[10.1016/0034-4257\(91\)90017-Z](https://doi.org/10.1016/0034-4257(91)90017-Z).
- Grier, C. G., and S. W. Running, 1977: Leaf area of mature northwestern coniferous forests: Relation to site water balance. *Ecology*, **58**, 893–899, doi:[10.2307/1936225](https://doi.org/10.2307/1936225).
- Guanter, L., C. Frankenberg, A. Dudhia, P. E. Lewis, J. Gómez-Dans, A. Kuze, H. Suto, and R. G. Grainger, 2012: Retrieval and global assessment of terrestrial chlorophyll fluorescence from GOSAT space measurements. *Remote Sens. Environ.*, **121**, 236–251, doi:[10.1016/j.rse.2012.02.006](https://doi.org/10.1016/j.rse.2012.02.006).
- Hilker, T., and Coauthors, 2014: Vegetation dynamics and rainfall sensitivity of the Amazon. *Proc. Natl. Acad. Sci. USA*, **111**, 16 041–16 046, doi:[10.1073/pnas.1404870111](https://doi.org/10.1073/pnas.1404870111).
- Holben, B. N., 1986: Characteristics of maximum-value composite images from temporal AVHRR data. *Int. J. Remote Sens.*, **7**, 1417–1434, doi:[10.1080/01431168608948945](https://doi.org/10.1080/01431168608948945).
- Huete, A., K. Didan, T. Miura, E. Rodriguez, X. Gao, and L. Ferreira, 2002: Overview of the radiometric and biophysical performance of the MODIS vegetation indices. *Remote Sens. Environ.*, **83**, 195–213, doi:[10.1016/S0034-4257\(02\)00096-2](https://doi.org/10.1016/S0034-4257(02)00096-2).
- Jasechko, S., Z. D. Sharp, J. J. Gibson, S. J. Birks, Y. Yi, and P. J. Fawcett, 2013: Terrestrial water fluxes dominated by transpiration. *Nature*, **496**, 347–350, doi:[10.1038/nature11983](https://doi.org/10.1038/nature11983).
- Jolly, W. M., R. Nemani, and S. W. Running, 2005: A generalized, bioclimatic index to predict foliar phenology in response to climate. *Global Change Biol.*, **11**, 619–632, doi:[10.1111/j.1365-2486.2005.00930.x](https://doi.org/10.1111/j.1365-2486.2005.00930.x).
- Jones, P., and I. Harris, 2013: CRU TS3.21: Climatic Research Unit (CRU) Time Series (TS) version 3.21 of high resolution gridded data of month-by-month variation in climate (Jan. 1901–Dec. 2012). NCAS British Atmospheric Data Centre, accessed 15 July 2016, doi:[10.5285/D0E1585D-3417-485F-87AE-4FCECF10A992](https://doi.org/10.5285/D0E1585D-3417-485F-87AE-4FCECF10A992).
- Jung, M., and Coauthors, 2011: Global patterns of land-atmosphere fluxes of carbon dioxide, latent heat, and sensible heat derived from eddy covariance, satellite, and meteorological observations. *J. Geophys. Res.*, **116**, G00J07, doi:[10.1029/2010JG001566](https://doi.org/10.1029/2010JG001566).
- Kottek, M., J. Grieser, C. Beck, B. Rudolf, and F. Rubel, 2006: World map of the Köppen-Geiger climate classification updated. *Meteor. Z.*, **15**, 259–264, doi:[10.1127/0941-2948/2006/0130](https://doi.org/10.1127/0941-2948/2006/0130).
- Koven, C. D., 2013: Boreal carbon loss due to poleward shift in low-carbon ecosystems. *Nat. Geosci.*, **6**, 452–456, doi:[10.1038/ngeo1801](https://doi.org/10.1038/ngeo1801).
- Lejenäs, H., and H. Økland, 1983: Characteristics of northern hemisphere blocking as determined from a long time series of observational data. *Tellus*, **35A**, 350–362, doi:[10.3402/tellusa.v35i5.11446](https://doi.org/10.3402/tellusa.v35i5.11446).
- Levis, S., 2010: Modeling vegetation and land use in models of the Earth system. *Wiley Interdiscip. Rev.: Climate Change*, **1**, 840–856, doi:[10.1002/wcc.83](https://doi.org/10.1002/wcc.83).
- Lugo, A. E., S. L. Brown, R. Dodson, T. S. Smith, and H. H. Shugart, 1999: The Holdridge life zones of the conterminous United States in relation to ecosystem mapping. *J. Biogeogr.*, **26**, 1025–1038, doi:[10.1046/j.1365-2699.1999.00329.x](https://doi.org/10.1046/j.1365-2699.1999.00329.x).
- Luo, Y. Q., and Coauthors, 2012: A framework for benchmarking land models. *Biogeosciences*, **9**, 3857–3874, doi:[10.5194/bg-9-3857-2012](https://doi.org/10.5194/bg-9-3857-2012).
- McDowell, N. G., 2011: Mechanisms linking drought, hydraulics, carbon metabolism, and vegetation mortality. *Plant Physiol.*, **155**, 1051–1059, doi:[10.1104/pp.110.170704](https://doi.org/10.1104/pp.110.170704).
- Metzger, M. J., R. G. H. Bunce, R. H. G. Jongman, R. Sayre, A. Trabucco, and R. Zomer, 2013: A high-resolution bioclimatic map of the world: A unifying framework for global biodiversity research and monitoring. *Global Ecol. Biogeogr.*, **22**, 630–638, doi:[10.1111/geb.12022](https://doi.org/10.1111/geb.12022).
- Mu, Q., F. A. Heinsch, M. Zhao, and S. W. Running, 2007: Development of a global evapotranspiration algorithm based on MODIS and global meteorology data. *Remote Sens. Environ.*, **111**, 519–536, doi:[10.1016/j.rse.2007.04.015](https://doi.org/10.1016/j.rse.2007.04.015).
- Myneni, R., F. Hall, P. Sellers, and A. Marshak, 1995: The interpretation of spectral vegetation indexes. *IEEE Trans. Geosci. Remote Sens.*, **33**, 481–486.
- , and Coauthors, 2002: Global products of vegetation leaf area and fraction absorbed PAR from year one of MODIS data. *Remote Sens. Environ.*, **83**, 214–231.
- Nemani, R. R., C. D. Keeling, H. Hashimoto, W. M. Jolly, S. C. Piper, C. J. Tucker, R. B. Myneni, and S. W. Running, 2003: Climate-driven increases in global terrestrial net primary production from 1982 to 1999. *Science*, **300**, 1560–1563, doi:[10.1126/science.1082750](https://doi.org/10.1126/science.1082750).
- O'Brien, R. M., 2007: A caution regarding rules of thumb for variance inflation factors. *Qual. Quant.*, **41**, 673–690, doi:[10.1007/s11135-006-9018-6](https://doi.org/10.1007/s11135-006-9018-6).
- Oleson, K. W., and Coauthors, 2010: Technical description of version 4.0 of the Community Land Model (CLM). NCAR

- Tech. Note NCAR/TN-478+STR, 266 pp. [Available online at [http://www.cesm.ucar.edu/models/ccsm4.0/clm/CLM4\\_Tech\\_Note.pdf](http://www.cesm.ucar.edu/models/ccsm4.0/clm/CLM4_Tech_Note.pdf).]
- Peel, M. C., B. L. Finlayson, and T. A. McMahon, 2007: Updated world map of the Köppen-Geiger climate classification. *Hydrol. Earth Syst. Sci.*, **11**, 1633–1644, doi:[10.5194/hessd-4-439-2007](https://doi.org/10.5194/hessd-4-439-2007).
- Pinzon, J. E., and C. J. Tucker, 2014: A non-stationary 1981–2012 AVHRR NDVI<sub>3g</sub> time series. *Remote Sens.*, **6**, 6929–6960, doi:[10.3390/rs6086929](https://doi.org/10.3390/rs6086929).
- Richardson, A. D., and Coauthors, 2010: Influence of spring and autumn phenological transitions on forest ecosystem productivity. *Philos. Trans. Roy. Soc. London*, **365B**, 3227–3246, doi:[10.1098/rstb.2010.0102](https://doi.org/10.1098/rstb.2010.0102).
- , T. F. Keenan, M. Migliavacca, Y. Ryu, O. Sonnentag, and M. Toomey, 2013: Climate change, phenology, and phenological control of vegetation feedbacks to the climate system. *Agric. For. Meteorol.*, **169**, 156–173, doi:[10.1016/j.agrformet.2012.09.012](https://doi.org/10.1016/j.agrformet.2012.09.012).
- Rubel, F., and M. Kotteck, 2010: Observed and projected climate shifts 1901–2100 depicted by world maps of the Köppen-Geiger climate classification. *Meteor. Z.*, **19**, 135–141, doi:[10.1127/0941-2948/2010/0430](https://doi.org/10.1127/0941-2948/2010/0430).
- Running, S. W., R. R. Nemani, F. A. Heinsch, M. Zhao, M. Reeves, and H. Hashimoto, 2004: A continuous satellite-derived measure of global terrestrial primary production. *BioScience*, **54**, 547–560, doi:[10.1641/0006-3568\(2004\)054\[0547:ACSMOG\]2.0.CO;2](https://doi.org/10.1641/0006-3568(2004)054[0547:ACSMOG]2.0.CO;2).
- Saatchi, S. S., and Coauthors, 2011: Benchmark map of forest carbon stocks in tropical regions across three continents. *Proc. Natl. Acad. Sci. USA*, **108**, 9899–9904, doi:[10.1073/pnas.1019576108](https://doi.org/10.1073/pnas.1019576108).
- Schlesinger, W. H., and S. Jasechko, 2014: Transpiration in the global water cycle. *Agric. For. Meteorol.*, **189–190**, 115–117, doi:[10.1016/j.agrformet.2014.01.011](https://doi.org/10.1016/j.agrformet.2014.01.011).
- Seddon, A. W. R., M. Macias-Fauria, P. R. Long, D. Benz, and K. J. Willis, 2016: Sensitivity of global terrestrial ecosystems to climate variability. *Nature*, **531**, 229–232, doi:[10.1038/nature16986](https://doi.org/10.1038/nature16986).
- Simard, M., N. Pinto, J. B. Fisher, and A. Baccini, 2011: Mapping forest canopy height globally with spaceborne lidar. *J. Geophys. Res.*, **116**, G04021, doi:[10.1029/2011JG001708](https://doi.org/10.1029/2011JG001708).
- Smith, G., A. C. Wilber, S. K. Gupta, and P. W. Stackhouse, 2002: Surface radiation budget and climate classification. *J. Climate*, **15**, 1175–1188, doi:[10.1175/1520-0442\(2002\)015<1175:SRBACC>2.0.CO;2](https://doi.org/10.1175/1520-0442(2002)015<1175:SRBACC>2.0.CO;2).
- , K. Priestley, N. Loeb, B. Wielicki, T. Charlock, P. Minnis, D. Doelling, and D. Rutan, 2011: Clouds and Earth Radiant Energy System (CERES), a review: Past, present and future. *Adv. Space Res.*, **48**, 254–263, doi:[10.1016/j.asr.2011.03.009](https://doi.org/10.1016/j.asr.2011.03.009).
- Solano, R., K. Didan, A. Jacobson, and A. Huete, 2010: MODIS vegetation indices (MOD13) C5 user's guide. The University of Arizona Terrestrial Biophysics and Remote Sensing Laboratory Rep., 42 pp. [Available online at <https://www.ctahr.hawaii.edu/grem/modis-ug.pdf>.]
- Sprugel, D. G., M. G. Ryan, J. Brooks, K. Vogt, and T. A. Martin, 1995: Respiration from the organ level to the stand. *Resource Physiology of Conifers*, W. Smith and T. Hinckley, Eds., Academic Press, 255–299.
- Takala, M., K. Luojus, J. Pulliainen, C. Derksen, J. Lemmetyinen, J.-P. Kärnä, J. Koskinen, and B. Bojkov, 2011: Estimating Northern Hemisphere snow water equivalent for climate research through assimilation of space-borne radiometer data and ground-based measurements. *Remote Sens. Environ.*, **115**, 3517–3529, doi:[10.1016/j.rse.2011.08.014](https://doi.org/10.1016/j.rse.2011.08.014).
- Whittaker, R. H., 1962: Classification of natural communities. *Bot. Rev.*, **28**, 1–239, doi:[10.1007/BF02860872](https://doi.org/10.1007/BF02860872).
- , 1970: *Communities and Ecosystems*. Macmillan, 162 pp.
- Wu, D., X. Zhao, S. Liang, T. Zhou, K. Huang, B. Tang, and W. Zhao, 2015: Time-lag effects of global vegetation responses to climate change. *Global Change Biol.*, **21**, 3520–3531, doi:[10.1111/gcb.12945](https://doi.org/10.1111/gcb.12945).
- Xiao, J., and Coauthors, 2011: Assessing net ecosystem carbon exchange of U.S. terrestrial ecosystems by integrating eddy covariance flux measurements and satellite observations. *Agric. For. Meteorol.*, **151**, 60–69, doi:[10.1016/j.agrformet.2010.09.002](https://doi.org/10.1016/j.agrformet.2010.09.002).
- Xu, G., and Coauthors, 2014: Changes in vegetation growth dynamics and relations with climate over China's landmass from 1982 to 2011. *Remote Sens.*, **6**, 3263–3283, doi:[10.3390/rs6043263](https://doi.org/10.3390/rs6043263).
- Zhang, T., P. W. Stackhouse, S. K. Gupta, S. J. Cox, J. C. Mikovitz, and L. M. Hinkelman, 2013: The validation of the GEWEX SRB surface shortwave flux data products using BSRN measurements: A systematic quality control, production and application approach. *J. Quant. Spectrosc. Radiat. Transfer*, **122**, 127–140, doi:[10.1016/j.jqsrt.2012.10.004](https://doi.org/10.1016/j.jqsrt.2012.10.004).
- Zhou, L., C. J. Tucker, R. K. Kaufmann, D. Slayback, N. V. Shabanov, and R. B. Myneni, 2001: Variations in northern vegetation activity inferred from satellite data of vegetation index during 1981 to 1999. *J. Geophys. Res.*, **106**, 20 069–20 083, doi:[10.1029/2000JD000115](https://doi.org/10.1029/2000JD000115).
- , R. K. Kaufmann, Y. Tian, R. B. Myneni, and C. J. Tucker, 2003: Relation between interannual variations in satellite measures of northern forest greenness and climate between 1982 and 1999. *J. Geophys. Res.*, **108**, 4004, doi:[10.1029/2002JD002510](https://doi.org/10.1029/2002JD002510).